Optica Applicata, Vol. LII, No. 1, 2022
DOI: 10.37190/oa220110

The study of temperature measurement based on the transmission of fixed wavelengths for helical long-period grating

YUNFENG BAI*, ZELONG HE, SUIHU DANG

Key Laboratory of Micro Nano Optoelectronic Devices and Intelligent Perception Systems, School of Electronic Information and Engineering, Yangtze Normal University, Chongqing, 408100, China

*Corresponding author: baiyunfeng@126.com

This research involves a fixed wavelength and dual-wavelength ratio temperature measurement for helical long-period grating. There are two resonant dips near 1475 and 1520 nm, with the pitch length 782 μm. The temperature sensitivity of resonance wavelengths is about 0.06 nm/°C. Both theoretical simulation and experiment results show that the transmission of a fixed wavelength linearly changes with the temperature. It has a high application value for measuring temperature. Besides, the dual-wavelength ratio is studied to eliminate the influence of light source. The temperature sensitivity of transmission intensity ratio of $I_{1469.6nm}/I_0$ and $I_{1469.6nm}/I_{1526.5nm}$ are about 1.0076/°C and 0.0155/°C, respectively, so the dual-wavelength ratio is more practical. And the 0.0155 times intensity change could be much more easily measured than the 0.06 nm wavelength change for each degree Celsius. So the dual-wavelength ratio of the helical long-period gratings is very suitable for temperature sensors.

Keywords: helical long-period grating, fixed wavelength, dual-wavelength ratio, temperature sensor.

1. Introduction

Long-period fiber grating (LPFG) has significant resonant dips caused by the coupling between guided fundamental mode and the forward-propagating cladding modes. LPFG has significant practical applications in optical fiber communication and fiber sensing field [1–3]. The helically twisted long-period fiber grating (H-LPFG) has periodic helical refractive index modulation on the axial and angle. H-LPFG is easy to process and does not need photosensitivity and doping for the fabrication of fiber gratings. H-LPFG is mainly applied to measure the twist rate [4–6], the refractive index [7], the applied stress [8], the temperature [8–11], and generate orbital angular momentum [12–17].

The fiber gratings are mainly utilized as the wavelength modulation sensors [1–11]. Edge filtering is applied to convert the wavelength change to intensity [18–20]. The accuracy of edge filtering is affected by the linearity and slope of the filter edge. Meanwhile, the measurement range of edge filtering is relatively small, and it imperatively needs a stable intensity light source.

In this paper, two neighboring resonance dips, which generate from the four-order coupling between the fundamental mode and the $LP_{1,10}$ cladding mode, have been studied. The wavelength responsivities of two resonance dips with temperature are measured. The resonance wavelengths show linear change with temperature, and the slopes are 62 and 59 pm/°C, respectively. The transmission responsivities of a fixed wavelength with temperature are studied. The theoretical simulation and experiment results show that the transmission of fixed wavelength changes linearly with temperature. The temperature sensitivity of transmission intensity ratio of $I_{1469.6nm}/I_0$ is about 1.0076/°C. Besides, to eliminate the influence of light source, the dual-wavelength ratio is deduced, and the experimental results show its linear change with temperature. The temperature sensitivity of transmission intensity ratio of $I_{1469.6nm}/I_{1526.5nm}$ is about 0.0155/°C. It has great potential applications in temperature sensors.

2. Fabrication of H-LPFG

The single-mode fiber is spiral by a welding machine (Fujikura FSM-100p+). Firstly, the electrode discharge and motor are calibrated. The stepping-motor selects the sweep model, and the stepping speed is 0.063 μm/ms. ZR motor rotates clockwise, and the rotation speed is 0.029°/ms. The electrode discharge power is –60bit relative to the calibration power, the electrode gap is 3 mm, and the running time is 200000 ms. As shown in Fig. 1, the fiber core, cladding, and surface morphology of the H-LPFG have nearly no change under a microscope (Olympus CX23).

Fig. 1. Photograph of the H-LPFG with a microscope.

The grating pitch of H-LPFG can be calculated by

$$\Lambda = 360\frac{V}{\theta} \tag{1}$$

where V is the stepping speed of a sweep mode, θ is the rotation speed of the ZR motor, Λ is the pitch length of the H-LPFG. The grating pitch of the H-LPFG is 782 μm, and the total length of the H-LPFG is about 12 mm.

3. Experimental results and discussions

A spectrometer (Yokogawa-AQ6370D) is used to measure the transmission spectrum at different temperatures as shown in Fig. 2. There are two resonant dips near 1475 and 1520 nm. And the dip1 decreases but the dip2 increases with increasing temperature.

According to the long-period fiber grating coupled-mode theory [21, 22], if the *n*-order harmonic is considered, the phase-matching condition for the single-helix H-LPFG can be described as [23],

$$n_{\mathrm{N}} = n_{\mathrm{F}} - \frac{n\lambda}{\Lambda} \tag{2}$$

where n is the harmonic order number, n_{F} and n_{N} are the effective refractive index of the fundamental mode and the coupled m-th cladding modes. λ is the resonant wavelength of the H-LPFG. The refractive indexes of the core and cladding are 1.4628 and 1.4573.

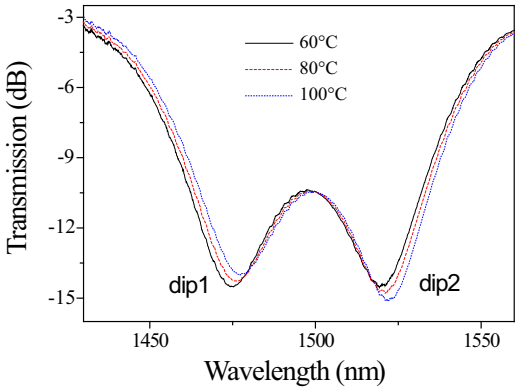

Fig. 2. The transmission spectrum of the H-LPFG with different temperatures.

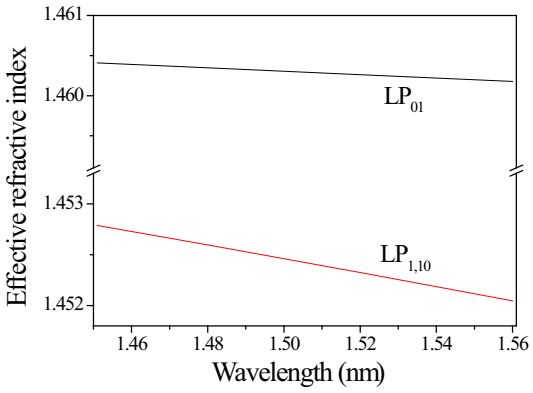

Fig. 3. The relationship between the effective refractive index and wavelength.

Basing on the phase-matching condition, Eq. (2), and theoretical calculation effective refractive index (as shown in Fig. 3), both dip1 and dip2 are four-order coupling between the fundamental mode and $LP_{1,10}$ cladding mode. The design wavelength is 1.51 μm for dip1 and 1.55 μm for dip2. But the design wavelengths do not agree with the experimental results of 1.475 and 1.52 μm for dip1 and dip2 separately. The relationship between resonant wavelength and design wavelength can be described as follows [24]:

$$n\lambda_{\mathrm{res}} = \frac{1}{1-(\sigma_{11}-\sigma_{22})\dfrac{\Lambda}{2\pi}}\lambda_{\mathrm{D}} \tag{3}$$

where σ_{11} and σ_{22} are DC coupling coefficients of the fundamental mode and the coupled m-th cladding mode, respectively; λ_{D} is the design wavelength, λ_{res} is the resonant wavelength. Based on Eq. (3), resonant wavelength λ_{res} and design wavelength λ_{D} are different, and the λ_{res} is usually smaller than λ_{D} when there are n-order harmonic.

The effective refractive index difference of the single-mode fiber between fiber core and $LP_{1,10}$ cladding mode are 0.0077 and 0.00797 for dip1 and dip2. The effective refractive index difference of the H-LPFG can be worked out by Eq. (2), and the values are 0.0075 and 0.0078 for dip1 and dip2 separately. The refractive index changes of the fiber core and cladding are nearly the same.

The wavelength responsivities of the H-LPFG with the temperature are measured by the broadband light source and optical spectrum analyzer. Temperature increases from 60 to 150°C, and the transmission spectrum is measured every 10°C rise. The results are shown in Fig. 4. The resonant wavelengths show a linear increase as the temperature goes up. The slopes are 62 pm/°C for dip1 and 59 pm/°C for dip2, same with the temperature measurement accuracy of ordinary LPFG [8].

The transmission responsivities of resonance wavelength with the temperature are also studied (as shown in Fig. 5). The transmission of resonance wavelengths also shows linearly with temperature. It agrees with Ng's report [25]. But this is useless for

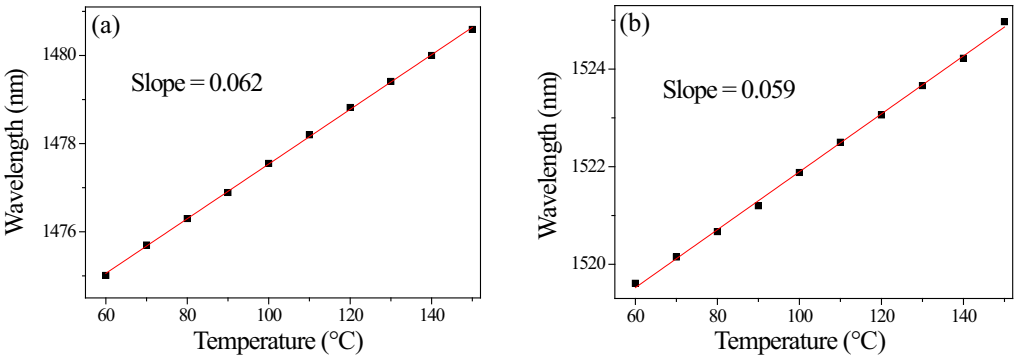

Fig. 4. Resonance wavelength *vs*. temperature: (**a**) dip1 and (**b**) dip2. Black squares are the measurement data, and the red line is linear fitting.

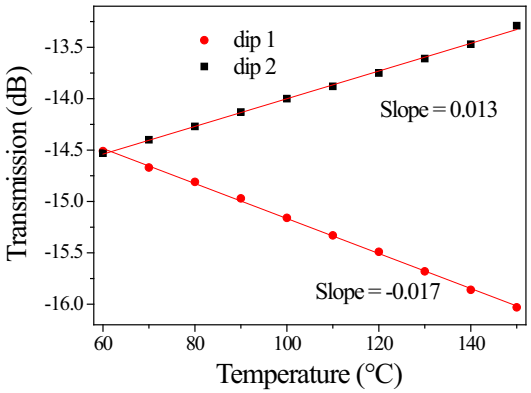

Fig. 5. Transmission of resonance wavelength *vs*. temperature.

simple temperature measurement or increasing the accuracy. So we consider choosing a fixed wavelength to measure the relationship between the transmission and temperature.

The transmission spectrum of the H-LPFG, which can be obtained from a standard coupled-mode theory [24, 26].

$$A = \cos^2\left(\sqrt{k^2+\hat{\sigma}^2}\, z\right) + \frac{\hat{\sigma}^2}{k^2+\hat{\sigma}^2}\sin^2\left(\sqrt{k^2+\hat{\sigma}^2}\, z\right) \tag{4}$$

$$\hat{\sigma} = \delta + \frac{\sigma_{11}-\sigma_{22}}{2} \tag{5}$$

$$\delta = \pi\Delta n_{\text{eff}}\left(\frac{1}{4\lambda} - \frac{1}{\lambda_{\text{D}}}\right) \tag{6}$$

where A is the transmission rate, DC is a self-coupling coefficient, k is an AC coupling coefficient, δ is detuning, λ is wavelength, z is the length of H-LPFG, n_1 and n_2 are the refractive index of the fiber core and the cladding, n_{eff} is the effective refractive index of the fundamental mode, $\sigma(z)$ is the slowly varying envelope of the grating. The expression of σ_{11}, k, and σ_{22} can be found in [26]. The thermo-optic coefficients of the fiber core and the cladding are 6.45×10^{-6}/°C and 6.34×10^{-6}/°C. The coefficient of thermal expansion is 5.5×10^{-7}/°C. The coefficient 4 in Eq. (6) comes from four-order coupling between the fundamental mode and $LP_{1,10}$ cladding mode.

The transmission of calculated and measured results at 1469.6 nm for the H-LPFG are shown in Fig. 6**a**. Both the measured results and simulation show there is a graded trend before 60°C, the transmission has a linear relation with the temperature after 60°C, and they are approximately parallel to each other. There is about a 3.5 dB difference between the measured results and the simulation, which might be caused by a coupling loss. As shown in Fig. 6**b**, the transmission of $\lambda_{1469.6\text{nm}}$ and $\lambda_{1526.5\text{nm}}$ change linearly with temperature. The sensitivity of transmission intensity ratio $I_{1469.6\text{nm}}/I_0$ and

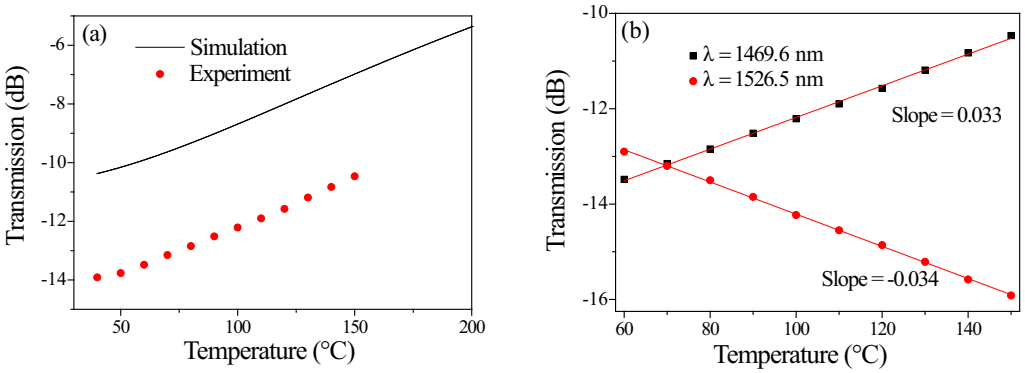

Fig. 6. (**a**) Thermal effects on the transmission of the H-LPFG with fixed wavelength at 1469.6 nm. (**b**) Transmission of fixed wavelength *vs*. temperature. The solid circles and solid squares are the measurement data, and the lines are a linear fitting.

$I_{1526.5\text{nm}}/I_0$ are about 1.0076/°C and 0.9922/°C. According to the fitting process, the DC self-coupling coefficient increases as the temperature increases at $I_{1469.6\text{nm}}$, so the intensity ratio $I_{1469.6\text{nm}}/I_0$ is greater than one. On the contrary, the DC self-coupling coefficient decreases as the temperature increases at $I_{1526.5\text{nm}}$, so the intensity ratio $I_{1526.5\text{nm}}/I_0$ is less than one. It provides a very competitive method of using a fixed wavelength transmission to measure temperature. But this measurement is affected by the incident intensity fluctuations.

The measured transmission varies with temperature and can be expressed as,

$$\frac{\mathrm{d}\left[10\lg(I/I_0)\right]}{\mathrm{d}T} = \frac{10\,\mathrm{d}(\lg A)}{\mathrm{d}T} \approx c \tag{7}$$

where I_0 is the incident intensity of the fundamental mode, I is the transmission intensity of the fundamental mode.

The dual-wavelength ratio is proposed to eliminate the influence of the light source. Two wavelengths are selected, and the corresponding incident intensity and transmission intensity are I_{10}, I_{20}, I_1, and I_2, respectively. Then the ratio of fixed dual-wavelength transmission intensity varies with temperature,

$$\frac{\mathrm{d}\left[10\lg\dfrac{I_1}{I_2}\right]}{\mathrm{d}T} = \frac{\mathrm{d}\left[10\lg\dfrac{I_1}{I_2}\dfrac{I_{10}}{I_{20}}\right]}{\mathrm{d}T} = \frac{\mathrm{d}\left[10\lg\dfrac{I_1}{I_{10}} - 10\lg\dfrac{I_2}{I_{20}}\right]}{\mathrm{d}T} = \frac{10\,\mathrm{d}(\lg A_1)}{\mathrm{d}T} - \frac{10\,\mathrm{d}(\lg A_2)}{\mathrm{d}T} \tag{8}$$

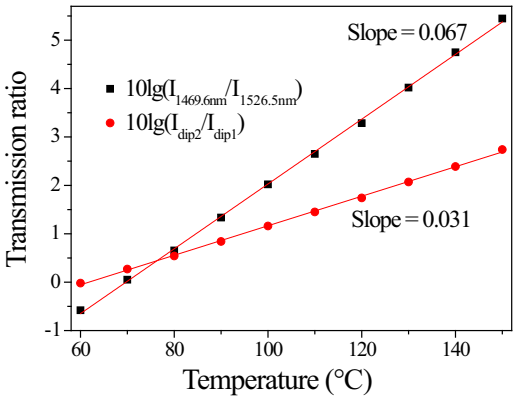

Fig. 7. $10\lg(I_{1469.6\text{nm}}/I_{1526.5\text{nm}})$ and $10\lg(I_{\text{dip2}}/I_{\text{dip1}})$ *vs.* temperature.

According to Eq. (8), $\mathrm{d}(\lg A_1)/\mathrm{d}T$ and $\mathrm{d}(\lg A_2)/\mathrm{d}T$ should have opposite signs, then the absolute value of Eq. (8) is the biggest. The wavelengths 1469.6 and 1526.5 nm located at both sides of different resonance dips are chosen. Besides, selecting two fixed wavelengths on both sides of the same resonance dip also satisfies Eq. (8).

As shown in Fig. 7, experimental results show that the fixed dual-wavelength ratio linearly changes with temperature, and the linearity is good. It indicates that using the above H-LPFG and two narrowband filters or two fiber Bragg gratings can measure temperature.

The temperature sensitivity of transmission intensity ratio of $I_{1469.6\text{nm}}/I_{1526.5\text{nm}}$ is about 0.0155/°C, which should be much easier to measure than the wavelength responsivities 0.06 nm/°C. So the temperature sensitivity of the dual-wavelength ratio can much bigger than the wavelength modulation sensor with an appropriate light source and detector. Although the light source used in our experiment is a broadband light source, we recommend choosing the cheaper LED when making the equipment. The light source emits natural light, and the influence of polarized light on the measurement is not considered. Moreover, in the experiment, we have bent and extruded the single-mode fiber, which has almost no effect on the measurement results. So it has great potential applications in temperature sensors.

4. Conclusion

In conclusion, this research presents a fixed wavelength and dual-wavelength ratio temperature measurement based on H-LPFG. Both theoretical simulation and experiment results show that the transmission of fixed wavelength changes linearly with temperature. Besides, the dual-wavelength ratio is applied to eliminate the influence of the light source. It provided a new way to high precision temperature measurement at a low cost. The work has magnificent practical applications in temperature sensors.

Funding
The work was supported by the Science and Technology Research Program of Chongqing Education Commission of China (KJQN20200142) and (KJZDM202001401). And by the University Innovation Research Group of Shale Gas Optical Fiber Intelligent Sensing Technology (CXQT20027).

References

[1] VENGSARKAR A.M., LEMAIRE P.J., JUDKINS J.B., BHATIA V., ERDOGAN T., SIPE J.E., *Long-period fiber gratings as band-rejection filters*, Journal of Lightwave Technology **14**(1), 1996, pp. 58–65, DOI: 10.1109/50.476137.
[2] BHATIA V., VENGSARKAR A.M., *Optical fiber long-period grating sensors*, Optics Letters **21**(9), 1996, pp. 692–694, DOI: 10.1364/OL.21.000692.
[3] SHU X.W., ZHANG L., BENNION I., *Sensitivity characteristics of long-period fiber gratings*, Journal of Lightwave Technology **20**(2), 2002, pp. 255–266, DOI: 10.1109/50.983240.
[4] GAO R., JIANG Y., JIANG L., *Multi-phase-shifted helical long period fiber grating based temperature-insensitive optical twist sensor*, Optics Express **22**(13), 2014, pp. 15697–15709, DOI: 10.1364/OE.22.015697.
[5] ZHANG L., LIU Y., ZHAO Y., WANG T., *High sensitivity twist sensor based on helical long-period grating written in two-mode fiber*, IEEE Photonics Technology Letters **28**(15), 2016, pp. 1629–1632, DOI: 10.1109/LPT.2016.2555326.
[6] ZHANG H.L., ZHANG W.G., CHEN L., XIE Z.D., ZHANG Z., YAN T.Y., WANG B., *Bidirectional torsion sensor based on a pair of helical long-period fiber gratings*, IEEE Photonics Technology Letters **28**(15), 2016, pp. 1700–1702, DOI: 10.1109/LPT.2016.2533478.
[7] WANG P., LI H., *Helical long-period grating formed in a thinned fiber and its application to a refractometric sensor*, Applied Optics **55**(6), 2016, pp. 1430–1434, DOI: 10.1364/AO.55.001430.
[8] SUN B., WEI W., LIAO C.R., ZHANG L., ZHANG Z.X., CHEN M.Y., WANG Y.P., *Automatic arc discharge-induced helical long period fiber gratings and its sensing applications*, IEEE Photonics Technology Letters **29**(11), 2017, pp. 873–876, DOI: 10.1109/LPT.2017.2693361.
[9] KOPP V.I., CHURIKOV V.M., ZHANG G., SINGER J., DRAPER C.W., CHAO N., NEUGROSCHL D., GENACK A.Z., *Single- and double-helix chiral fiber sensors*, Journal of the Optical Society of America B **24**(10), 2007, pp. A48–A52, DOI: 10.1364/JOSAB.24.000A48.
[10] XIAN L.L., WANG P., LI H.P., *Power-interrogated and simultaneous measurement of temperature and torsion using paired helical long-period fiber gratings with opposite helicities*, Optics Express **22**(17), 2014, pp. 20260–20267, DOI: 10.1364/OE.22.020260.
[11] XU C.C., JIANG C., LIU Y.Q., *High diffraction order cladding modes of helical long-period gratings inscribed by CO_2 laser*, Applied Optics **59**(10), 2020, pp. 3086–3092, DOI: 10.1364/AO.387578.
[12] WONG G.K.L., KANG M.S., LEE H.W., BIANCALANA F., CONTI C., WEISS T., RUSSELL P.ST.J., *Excitation of orbital angular momentum resonances in helically twisted photonic crystal fiber*, Science. **337**(6093), 2012, pp. 446–449, DOI: 10.1126/science.1223824.
[13] FU C.L., LIU S., BAI Z.Y., HE J., LIAO C.R., WANG Y., LI Z.L., ZHANG Y., YANG K.M., YU B., WANG Y.P., *Orbital angular momentum mode converter based on helical long period fiber grating inscribed by hydrogen–oxygen flame*, Journal of Lightwave Technology **36**(9), 2018, pp. 1683–1688, DOI: 10.1109/JLT.2017.2787120.
[14] ZHANG Y., BAI Z.Y., FU C.L., LIU S., TANG J., YU J., LIAO C.R., WANG Y., HE J., WANG Y.P., *Polarization-independent orbital angular momentum generator based on a chiral fiber grating*, Optics Letters **44**(1), 2019, pp. 61–64, DOI: 10.1364/OL.44.000061.
[15] FU C.L., WANG Y.P., BAI Z.Y., LIU S., ZHANG Y., LI Z.L., *Twist-direction-dependent orbital angular momentum generator based on inflation-assisted helical photonic crystal fiber*, Optics Letters **44**(2), 2019, pp. 459–462, DOI: 10.1364/OL.44.000459.

[16] Zhao H., Wang P., Yamakawa T., Li H.P., *All-fiber second-order orbital angular momentum generator based on a single-helix helical fiber grating*, Optics Letters **44**(21), 2019, pp. 5370–5373, DOI: 10.1364/OL.44.005370.

[17] He X.D., Tu J.J., Wu X.W., Gao S., Shen L., Hao C.L., Feng Y.H., Ping W.L., Li Z.H., *All-fiber third-order orbital angular momentum mode generation employing an asymmetric long-period fiber grating*, Optics Letters **45**(13), 2020, pp. 3621–3624, DOI: 10.1364/OL.394333.

[18] Melle S.M., Liu K., Measures R.M., *A passive wavelength demodulation system for guided-wave Bragg grating sensors*, IEEE Photonics Technology Letters **4**(5), 1992, pp. 516–518, DOI: 10.1109/68.136506.

[19] Davis M.A., Kersey A.D., *All-fibre Bragg grating strain-sensor demodulation technique using a wavelength division coupler*, Electronics Letters **30**(1), 1994, pp. 75–77, DOI: 10.1049/el:19940059.

[20] Sano Y., Yoshino T., *Fast optical wavelength interrogator employing arrayed waveguide grating for distributed fiber Bragg grating sensors*, Journal of Lightwave Technology **21**(1), 2003, pp. 132–139, DOI: 10.1109/JLT.2003.808620.

[21] Ivanov O.V., *Propagation and coupling of hybrid modes in twisted fibers*, Journal of the Optical Society of America A **22**(4), 2005, pp. 716–723, DOI: 10.1364/JOSAA.22.000716.

[22] Shvets G., Trendafilov S., Kopp V.I., Neugroschl D., Genack A.Z., *Polarization properties of chiral fiber gratings*, Journal of Optics A: Pure and Applied Optics **11**(7), 2009, article 074007, DOI: 10.1088/1464-4258/11/7/074007.

[23] Napiorkowski M., Urbanczyk W., *Role of symmetry in mode coupling in twisted microstructured optical fibers*, Optics Letters **43**(3), 2018, pp. 395–398, DOI: 10.1364/OL.43.000395.

[24] Erdogan T., *Fiber grating spectra*, Journal of Lightwave Technology **15**(8), 1997, pp. 1277–1294, DOI: 10.1109/50.618322.

[25] Ng M.N., Chiang K.S., *Thermal effects on the transmission spectra of long-period fiber gratings*, Optics Communications **208**(4–6), 2002, pp. 321–327, DOI: 10.1016/S0030-4018(02)01597-3.

[26] Erdogan T., *Cladding-mode resonances in short- and long-period fiber grating filters*, Journal of the Optical Society of America A **14**(8), 1997, pp. 1760–1773, DOI: 10.1364/JOSAA.14.001760.

Received March 6, 2021